Phonon Dispersion Curves by Raman Scattering in SiC, Polytypes 3C, 4H, 6H, 15R, and 21R†

D. W. FELDMAN, JAMES H. PARKER, JR., W. J. CHOYKE, AND LYLE PATRICK
Westinghouse Research Laboratories, Pittsburgh, Pennsylvania 15235
(Received 16 April 1968)

Phonon dispersion curves for SiC have been constructed from first-order Raman scattering data. The method used is a new one that exploits the existence of polytypes. Excitation by an argon ion laser made possible the observation of nine one-phonon lines in 4*H* SiC, 16 lines in 15*R*, and 14 lines in 21*R*. The symmetry type of each phonon mode was determined by polarization analysis, and the modes were further classified by the use of a standard large zone. The three groups of one-phonon lines, together with 15 lines previously reported for 6*H* SiC, were then all assigned to their positions in a single large-zone plot, to yield a set of SiC phonon dispersion curves comparable with those obtained for other materials by neutron diffraction. The results verify the existence of a common phonon spectrum for all SiC polytypes in the axial direction. Longitudinal and transverse acoustic velocities are obtained from the dispersion curves, and are in good agreement with experimental values. Thus, optic modes in polytypes give information on acoustic properties. All SiC polytypes have in common a set of strong modes in which the Si and C sublattices vibrate against each other. The anisotropy of one of these modes varies with polytype in the same way as the *c/a* axial ratios. Both the anisotropy and the *c/a* ratio are related empirically to the percentage of hexagonal planes in the polytype stacking arrangement.

I. INTRODUCTION

A NEW method of obtaining phonon dispersion curves is based on the existence of polytypes. SiC polytypes differ in the stacking order of atomic planes,[1] but are alike in many physical properties. Measurements on a polytype often yield results that are determined partly by the properties common to all polytypes, and partly by the unique structure of the polytype on which the measurements are made. An example is the recently reported[2] first-order Raman spectrum of 6*H* SiC. The property assumed to be common to all polytypes is, in this case, the phonon spectrum in the axial direction.[3] Most of the lines in the Raman spectrum are, nevertheless, characteristic of the 6*H* structure, which determines the points of the common spectrum that are accessible to Raman measurements. The relationship of the Raman spectrum to the phonon spectrum is clear from a large-zone point of view, which permits the assignment of Raman frequencies to positions on dispersion curves, even though these modes have zero wave-vectors (approximately) in the Brillouin zone.

The existence of a common SiC phonon spectrum (within 2%) is verified by the measurements on 4*H*, 15*R*, and 21*R* polytypes reported here. Because of the weakness of many of the Raman lines, the use of an argon ion laser for excitation was an important factor in the observation of 9 lines in 4*H* SiC, 16 lines in 15*R*, and 14 lines in 21*R*. The standard large zone makes it possible to compare frequencies measured in these different polytypes. It enables us to plot all the Raman data in a single figure, thus to obtain dispersion curves comparable, in completeness and accuracy, with those obtained for other materials by neutron diffraction (but for only one direction in momentum space). Each polytype contributes a characteristic set of points to the joint dispersion curves. The Raman scattering method can be applied to any material that has polytypic modifications, e.g., to ZnS, if sufficiently large single-polytype crystals can be grown.

Although Raman scattering gives the frequencies of optic modes only, the dispersion curves in the large zone comprise both optic and acoustic branches. From the latter we obtain acoustic velocities for both longitudinal and shear modes that are in good agreement with values measured by standard acoustic methods.

Long-wavelength vibrational modes in SiC polytypes are of two kinds, called "strong" and "weak" because of their very different infrared strengths.[4] The dispersion curves are constructed primarily from the weak modes. One of the strong modes has a small variation of frequency with phonon propagation direction, a variation that yields a measure of the crystal anisotropy. Thus, the dependence of anisotropy on polytype can be studied, and can be related, for example, to the deviation from the ideal *c/a* axial ratio. Both measures of anisotropy correlate well with a parameter that has proved useful in the analysis of other polytype materials, the parameter being obtained by a definition of the percentage of hexagonal layers in the polytype.

A summary of the essential properties of polytypes and large zones is given in Sec. II. The experimental results for polytypes 4*H*, 15*R*, and 21*R* are presented in separate parts in Sec. IV. The data from these polytypes are then combined with data previously given for 6*H* SiC to obtain the dispersion curves in Sec. V. Acoustic velocities are calculated from the dispersion curves, and are compared with experimental values. Finally, in

† This work was supported in part by the U. S. Air Force Materials Laboratory, Wright-Paterson Air Force Base, Ohio, under Contract No. F33615-68-C1267.

[1] A. R. Verma and P. Krishna, *Polymorphism and Polytypism in Crystals* (John Wiley & Sons, Inc., New York, 1966).

[2] D. W. Feldman, James H. Parker, Jr., W. J. Choyke, and Lyle Patrick, Phys. Rev. **170**, 698 (1968).

[3] Lyle Patrick, Phys. Rev. **167**, 809 (1968).

[4] Some quantitative comparisons are given in Ref. 3.

Sec. VI, the strong modes and the crystal anisotropy are discussed.

II. POLYTYPES AND LARGE ZONES

SiC polytypes have many atoms per unit cell, hence many first-order Raman lines, as indicated in Table I. The observed lines are first classified by symmetry type, which is determined by the use of polarized light excitation and polarization analysis of the scattered light. Further classification is based on a large-zone analysis, which also makes it possible to compare Raman lines in different polytypes. The required information on polytypes and large zones has been given in earlier papers, but the essentials will be summarized here.

Two of the polytypes we wish to compare, $4H$ and $6H$, are hexagonal ($P6_3mc$), and two, $15R$ and $21R$, are rhombohedral ($R3m$). In the Ramsdell designation, NH or NR, N is the number of atomic layers in the stacking unit; hence the lattice constant c_N is, to a good approximation, proportional to the number N in the Ramsdell symbol. The Brillouin zone boundary, in the axial direction, is at π/c_N for hexagonal polytypes, which have $2N$ atoms per unit cell, and at $3\pi/c_N$ for rhombohedral polytypes, which have $2N/3$ atoms per unit cell. In both cases we take the standard large-zone boundary at $q_{\max}=N\pi/c_N$, thereby reducing the number of phonon branches to six. Because c_N is proportional to N, the large zone has the same extension in q space for all polytypes. Thus, the reduced pseudomomentum coordinate $x=q/q_{\max}$ can be used to compare or correlate frequencies measured in different polytypes.

In each polytype, the modes active in first-order Raman scattering are long-wavelength modes in the Brillouin-zone picture, but are strung out along axial dispersion curves in the large-zone picture.[5] The strong modes, in which the Si and C sublattices vibrate against each other, remain at $x=0$ in the large zone, but the weak modes are assigned to positions $x\neq 0$ which are different for different polytypes. The special values of x in the large zone that are accessible to Raman scattering were given in Ref. 3, and are listed in Table I for the four polytypes discussed here. The usefulness of the large-zone concepts in the interpretation of polytype Raman spectra was demonstrated for $6H$ SiC in Ref. 2.

TABLE I. Raman-active modes and large-zone values of $x=q/q_{\max}$ for five polytypes. The zinc-blende ($3C$) Raman spectrum, with $x=0$ only, does not contribute to the phonon dispersion curves.

Ramsdell notation	Atoms per unit cell	Raman-active modes	Accessible values of x
$3C$	2	T_1	0
$4H$	8	$3A_1, 3E_1, 4E_2$	0, 0.5, 1
$6H$	12	$5A_1, 5E_1, 6E_2$	0, 0.33, 0.67, 1
$15R$	10	$9A_1, 9E$	0, 0.4, 0.8
$21R$	14	$13A_1, 13E$	0, 0.29, 0.57, 0.86

[5] From the Brillouin-zone point of view, modes of the same symmetry type are distinguished by their different intracell motions. Assigning a mode to a position $x=q/q_{\max}$ on the dispersion curves is equivalent to identifying its intracell motion.

III. SiC SAMPLES AND EXPERIMENTAL PROCEDURES

A. Polytype Specimens

The SiC samples were vapor-grown in a carbon-tube furnace[6] in which the product was largely $6H$ SiC. Small, pure polytype specimens of $4H$, $15R$, and $21R$ were occasionally found, but larger portions of these polytypes were always intergrown with $6H$ and/or other polytypes. The polytypes were identified by transmission Laue pictures, and, in n-type specimens, by their dichroism.[7] The selected specimens were reduced to pure polytype samples by grinding off the unwanted parts, after which the purity was verified by additional Laue photographs. It is clear that the first-order Raman lines, being sharp and characteristic, now provide another good method of polytype identification. The measurements were made on a single large specimen of each polytype, cut in the form of a rectangular parallelopiped, with the c axis normal to the largest face.

B. Experimental Procedures

The argon ion laser and associated equipment used for the $6H$ Raman measurements were described in Ref. 2. No changes were required by the substitution of polytypes with slightly different energy gaps.[8] The 4880 Å laser line was again used for excitation, and the samples were at room temperature for all measurements.

Polarized light was used to determine the symmetry types of the vibrational modes.[9] The method was discussed in detail for $6H$ SiC, and in references given there.[2] It requires observation of the Raman spectrum in several arrangements, with different propagation and polarization directions, each described by a four-letter symbol, e.g., $x(zx)y$, following the notation[10] of Damen *et al.*[11] The unequivocal identification of mode symmetry may also require intensity comparisons, because the finite acceptance angle of the monochromator sometimes permits strong lines to be recorded in an arrangement for which they should not appear.

The convenient phonon propagation directions were determined, as in $6H$ SiC, by the crystal cut. They were

[6] D. R. Hamilton, J. Electrochem. Soc. **105**, 735 (1958).
[7] E. Biedermann, Solid State Commun. **3**, 343 (1965).
[8] W. J. Choyke, D. R. Hamilton, and Lyle Patrick, Phys. Rev. **133**, A1163 (1964).
[9] R. Loudon, Advan. Phys. **13**, 423 (1964).
[10] The letters in the symbol refer to axes x, y, and z, fixed in the crystal, with z along the c axis. In the symbol $x(zx)y$, the part $x(--)y$ indicates that light incident in the x direction is scattered in the y direction. The part $-(zx)-$ indicates that incident and scattered light have polarization directions z and x, respectively.
[11] T. C. Damen, S. P. S. Porto, and B. Tell, Phys. Rev. **142**, 570 (1966).

$\theta=90°$ and 45°, where θ is the angle between the propagation vector and the crystal c axis.

IV. EXPERIMENTAL RESULTS

We consider only the first-order Raman lines, for which the criterion is a half-width of 4 cm^{-1} or less. Broader lines are observed, but are thought to be second-order. The SiC phonons active in first-order scattering have representations A_1, E_1, or E_2 in hexagonal polytypes, A_1 or E in rhombohedral. In both cases they fall into two distinct groups.[2,3] (1) The strong modes, at $x=0$ (strong in infrared absorption), have almost the same frequencies in all polytypes. They are longitudinal or transverse, and have energies that depend (slightly) on the angle θ between propagation vector and c axis.[9] This angular dependence will be considered in Sec. VI, where polytype anisotropy is discussed. (2) The weak modes, at $x\neq0$, are classified according to their atomic motions as axial ($\parallel$ to c) or planar ($\perp$ to c), the planar modes being double. The weak mode frequencies are characteristic of the polytype, and independent of the angle θ. It is these modes that are used to build the dispersion curves. They will be discussed separately for 4H, 15R, and 21R in this section, then combined in Sec. V.

Doublets are observed in the Raman spectra and give a measure of the energy discontinuities within the large zone. No Coulomb splitting of weak E_1 (or E) modes into longitudinal and transverse components has been observed, nor is it expected, in view of their small infrared strength. The only other degenerate representation, E_2, does not split because it is infrared inactive.

The procedure for identification of mode symmetry has been stated, but, in order to condense the presentation of data, it will not be illustrated. Instead, only one figure will be shown for each polytype, with the lines marked by their symmetry types as determined in separate experimental arrangements.

A. Polytype 4H

Polytype 4H, like 6H, has C_{6v} symmetry, and its Raman spectrum can be analyzed by the same procedures. It differs from 6H in the number of atoms per unit cell (8 instead of 12), and in the accessible values of $x=q/q_{max}$ (Table I). The long-wavelength normal modes of a hexagonal polytype are $N(A_1+B_1+E_1+E_2)$, with $N=4$ for 4H. The A_1 and E_1 modes appear at $x=0$ and 1 in the large zone,[3] strong modes at $x=0$, and weak modes at $x=1$. The B_1 and E_2 modes appear at $x=0.5$, doubled in number because of the energy discontinuity there, with B_1 modes Raman forbidden.

Figure 1 shows a Raman spectrum for 4H SiC without polarization analysis of the scattered light, in an arrangement chosen to display all allowed modes, A_1, E_1, and E_2. All the lines detected are shown except one weak component of an E_2 doublet at 196 cm^{-1} (position indicated by a bracketed $[E_2]$). The labels in Fig. 1 indicate the result of the symmetry analysis.

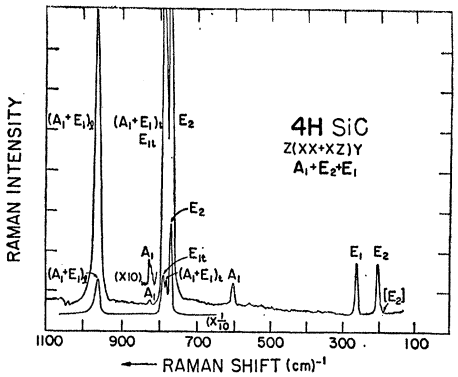

FIG. 1. Raman spectrum of 4H SiC, showing full range of the one-phonon-emission part, with a polarization arrangement chosen to show all Raman-active modes A_1, E_1, and E_2.

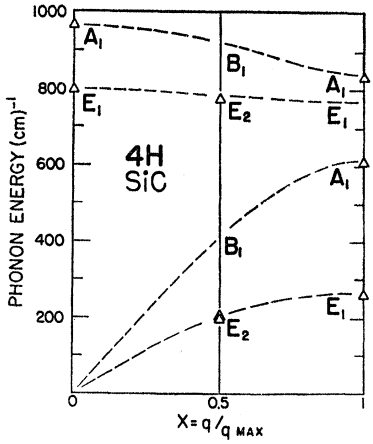

FIG. 2. Phonon dispersion curves, based on the 4H data in Table II. Energies and symmetries of the strong modes, at $x=0$, are appropriate for the propagation direction $\theta=0°$.

The assignment of all modes to positions in the large zone is unambiguous, and, for the weak modes, is indicated in Fig. 2 and Table II. Note that the phonon branches are not longitudinal and transverse, but axial and planar, as explained in Ref. 3. Only two expected lines were not observed (N.O. in Table II). The only doublets expected are two E_2 at $x=0.5$, and in one of

TABLE II. Energies (in cm^{-1}) of 4H weak phonon modes, with their representations, and assignments to values of $x=q/q_{max}$ in the large zone. They are listed in the order in which they are plotted in Fig. 2. B_1 modes are forbidden (F), and two of the expected modes have not been observed (N.O.).

Branch	$x=0.5$		$x=1$	
Axial optic	B_1	F	A_1	838
	B_1	F		
Planar optic	E_2	776	E_1	N.O.
	E_2	N.O.		
Axial acoustic	B_1	F	A_1	610
	B_1	F		
Planar acoustic	E_2	204	E_1	266
	E_2	196		

these a component is either unresolved or undetected. The remaining doublet has a splitting of 8 cm^{-1}, which is comparable with splittings previously observed in 6*H*.

Line intensities depend on the arrangement used, but frequencies do not, except for the slight angular dependence of the strong modes at $x=0$. The propagation angle θ is 45° in Fig. 1, hence two of the strong modes, being longitudinal or transverse, have mixed symmetry types, $(A_1+E_1)_l$ and $(A_1+E_1)_t$. The energies and representations shown for the modes at $x=0$ in Fig. 2 are appropriate for phonons propagating along the c axis, i.e., $\theta=0°$ (*ordinary* phonons). The strong modes are discussed further in Sec. VI.

The weak modes, at $x\neq 0$, are genuinely weak in infrared strength (A_1 or E_1) or infrared forbidden (E_2), but they show considerable variation in Raman intensity. For example, the three E_2 modes at 776, 204, and 196 cm^{-1} have intensities roughtly in the ratios 400:20:1.

B. Polytype 15*R*

Polytype 15*R* is rhombohedral (*R*3*m*), with point group symmetry C_{3v}. The symmetry is lower than that of hexagonal polytypes because the stacking sequence of atomic planes does not permit the screw displacement operation. A compatibility table shows that, under this reduction of symmetry, the axial modes A_1 and B_1 of C_{6v} both reduce to A_1 of C_{3v}, and the planar modes E_1 and E_2 of C_{6v} both reduce to E of C_{3v}. The Raman tensors for point group C_{3v} are given by Loudon.[9] Polytype 15*R* has 10 atoms per unit cell, and the normal modes are $10(A_1+E)$, all active in Raman scattering.

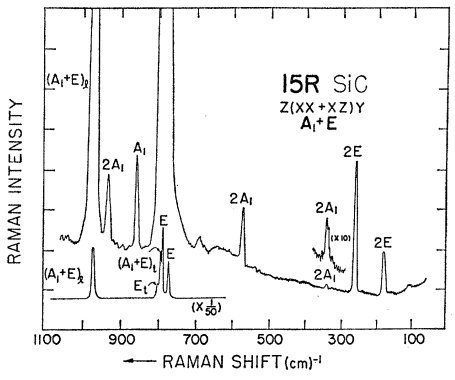

FIG. 3. Raman spectrum of 15*R* SiC, showing both A_1 and E modes. Doublets, shown as $2A_1$ and $2E$, are not resolved in this figure.

[12] The small energy discontinuities in the large zones of rhombohedral polytypes fall at multiples of $3\pi/c$ along the axial direction, but the points accessible to Raman scattering fall at multiples of $6\pi/c$. Hence rhombohedral polytypes, unlike hexagonal, have energy discontinuities at values of $x=q/q_{max}$ other than those listed in Table I. However, these additional discontinuities also have their origin in the very small inequivalencies of Si and C sites, and are therefore likely to be of the same magnitude as those accessible to measurement by Raman scattering.

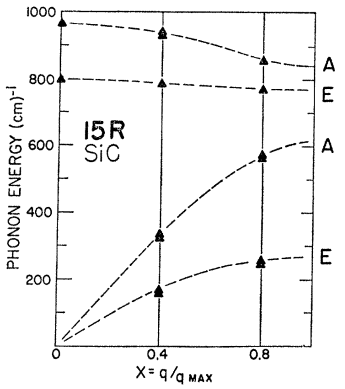

FIG. 4. Phonon dispersion curves, based on the 15*R* data in Table III.

A_1 and E modes now appear at all accessible values of x in the large zone,[12] namely, at $x=0$, 0.4, and 0.8.

Figure 3 shows a 15*R* Raman spectrum without polarization analysis of the scattered light, in an arrangement permitting both A_1 and E modes. In this figure, five lines are unresolved doublets, indicated by $2A_1$ or $2E$. The resolution of the doublets, and the identification of mode symmetry, were again done in other experimental arrangements (not shown), and the large-zone assignments are given in Fig. 4 and Table III. Because of the reduced symmetry of 15*R* SiC, the assignments to values of $x=q/q_{max}$ depend less on the symmetry analysis and more on the knowledge of the phonon spectrum previously obtained from 6*H* and 4*H* data. For example, to obtain a smooth planar optic branch in the joint dispersion curves, the E modes at 785 and 769 cm^{-1} must be assigned to $x=0.4$ and 0.8, respectively, rather than the reverse order.

Three expected lines were not observed (N.O. in Table III). They are all components of doublets, and may be either weak or unresolved. Splittings vary from 2 to 8 cm^{-1} in the five doublets recorded. The doublet 569 and 577 cm^{-1} on the axial acoustic branch at $x=0.8$ was observed by Ellis and Moss[13] in infrared absorption (but not resolved). Because the atomic motion is along

TABLE III. Energies (in cm^{-1}) of 15*R* weak phonon modes, and assignments to values of $x=q/q_{max}$ in the large zone. They are plotted in Fig. 4. Because the symmetry is C_{3v}, all axial modes are A_1, and all planar modes are E. In three cases, one of the doublet components was not observed (N.O.).

Branch	$x=0.4$	$x=0.8$
Axial optic (A_1)	938	860
	932	N.O.
Planar optic (E)	785	769
	N.O.	N.O.
Axial acoustic (A_1)	337	577
	331	569
Planar acoustic (E)	172	256
	167	254

[13] B. Ellis and T. S. Moss, Proc. Roy. Soc. (London) 299, 393 (1967).

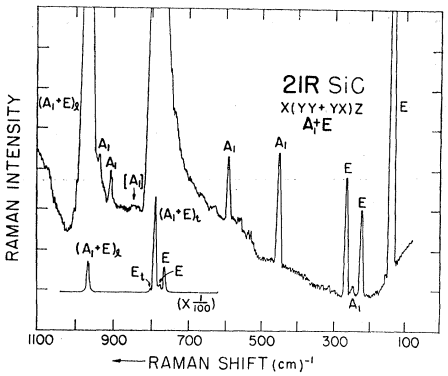

FIG. 5. Raman spectrum of 21R SiC, showing both A_1 and E modes. The second-order background is relatively high for this polytype.

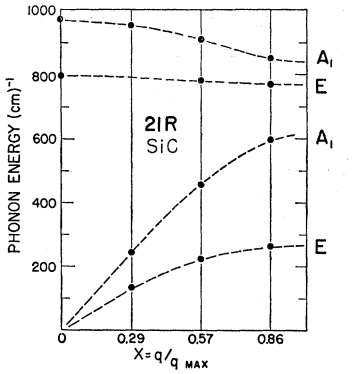

FIG. 6. Phonon dispersion curves based on the 21R data in Table IV.

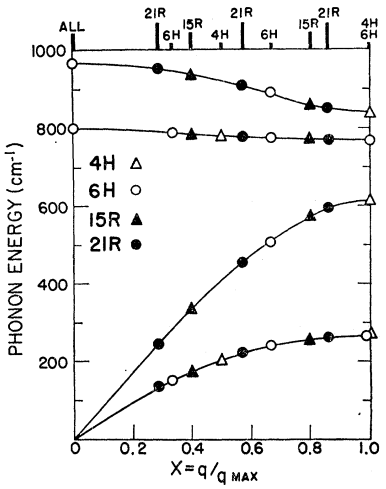

FIG. 7. Combined dispersion curves using data from four polytypes. For each polytype, the Raman accessible values of $x=q/q_{max}$ are marked at the top of the figure.

the axis, it is transverse for the extraordinary ray, and the doublet is, therefore, infrared-active.[3]

C. Polytype 21R

Polytype 21R has the same symmetry as 15R. It has 14 atoms per unit cell, and the normal modes are $14(A_1+E)$, all Raman-active, to be assigned to the large[14] zone at $x=0$, 0.29, 0.57, and 0.86.

Figure 5 shows all the observed lines except one whose position at 849 cm^{-1} is indicated by the bracketed $[A_1]$. The analysis is the same as for 15R, and the results are shown in Fig. 6 and Table IV. The assignment of E modes at 781 and 768 cm^{-1} to the planar optic branch is, again, the one that best fits the joint dispersion curves.

The ratio of first- to second-order Raman intensities varies from one polytype to another, and is rather low for 21R. Consequently, the second-order background is quite high in Fig. 5. Probably this is one reason why no doublets have been recorded, although 12 are predicted. Another possibility is that the 21R doublet splittings are too small to resolve. The higher polytypes have many modes and their large zones have many internal energy discontinuities. It seems reasonable that both line intensities and doublet splittings may decrease as their number increases. To make Table IV complete, and consistent with Tables II and III, there should be an additional entry of N.O. at each of the 12 positions. Except for these doublet components, all expected lines are observed but one.

V. SiC DISPERSION CURVES

A. Combined Raman Data

We can now test the assumption of a common phonon spectrum for SiC polytypes in the axial direction. We plot the combined data of polytypes 4H, 6H, 15R, and 21R, thus obtaining the joint dispersion curves of Fig. 7. Where a doublet was observed, it is represented by its average value, thereby eliminating the small discontinuities that are characteristic of the dispersion curves of individual polytypes. Where only one component of a doublet was recorded, our data indicates that it is not likely to differ from the desired average by more than 4 cm^{-1}. Not all the predicted Raman lines were found, but all the observed narrow lines, in all four polytypes, can be assigned to natural positions on the common dispersion curves. Large-zone assignments for the individual polytypes were made with these curves in mind, and are quite obvious for three of the four

[14] The values of $x=q/q_{max}$ for 21R are given by $6n/21$, with integral n.

TABLE IV. Energies (in cm^{-1}) of 21R weak phonon modes, and assignments to values of $x=q/q_{max}$ in the large zone. They are plotted in Fig. 6. Doublets are expected, but not observed, at each of the 12 positions. Hence, to be consistent with Tables II and III, there should be an additional 12 entries of N.O.

Branch	$x=0.29$	$x=0.57$	$x=0.86$
Axial optic (A_1)	949	908	849
Planar optic (E)	N.O.	781	768
Axial acoustic (A_1)	242	453	592
Planar acoustic (E)	132	219	260

branches. However, the assignment of modes to the relatively flat planar optic branch is somewhat less certain.

The only values of x at which we can compare phonon energies measured in different polytypes are $x=0$ and 1. The strong modes at $x=0$ are found in all polytypes, and, for the ordinary phonon, ($\theta=0°$), their frequencies are the same, within experimental uncertainty. Small differences that depend on the propagation angle θ will be considered in Sec. VI. At $x=1$, Raman-active modes are found only in the hexagonal polytypes, $4H$ and $6H$, and in the latter the two axial modes are forbidden (B_1). In polytype $4H$ the planar optic E_1 at $x=1$ was not observed, so the only comparison remaining is for the planar acoustic mode, which is listed at 266 cm^{-1} for $4H$, and 262 cm^{-1} for $6H$. The difference may not be significant, since experimental uncertainty is about 2 cm^{-1}. The modes being compared are a weakly infrared-active E_1 in $4H$, and an infrared-inactive E_2 in $6H$, but the symmetry difference is presumably irrelevant. Between $x=0$ and 1, the smoothness of the dispersion curves appears to verify the concept of a common phonon spectrum for all polytypes, within perhaps 2%.

B. Acoustic Velocities

From the acoustic branches of the large-zone dispersion curves we can obtain the velocities of sound waves propagating along the c axis, velocities that are, presumably, independent of polytype to a good approximation. Sound waves correspond to small values of x, and the points closest to $x=0$ in the Raman spectra are obtained from polytype $21R$. We use the $21R$ modes at $x=0.29$, namely, 242 and 132 cm^{-1}, to calculate longitudinal and shear velocities. A consideration of the accessible values of x shows that higher polytypes would give points still closer to $x=0$, e.g., in $33R$, Raman lines are expected for $x=6/33=0.18$.

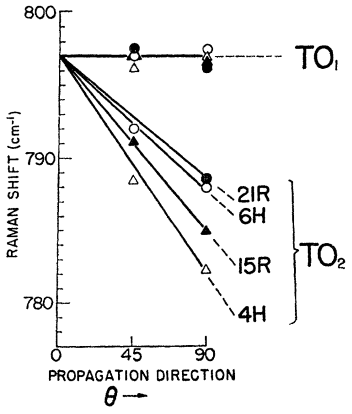

FIG. 8. Energies of the strong ($x=0$) transverse modes for four polytypes, and for propagation angles $\theta=45°$ and 90°. The mode TO_1 is planar, and does not vary with θ. The mode TO_2 is also planar, and degenerate with TO_1 for $\theta=0°$, but is axial, and has a lower energy for $\theta=90°$. The difference, TO_1-TO_2 at $\theta=90°$, is a measure of crystal anisotropy, and depends on polytype.

TABLE V. Comparison of measured sound velocities in SiC with those obtained from the acoustic branches of the large zone (specifically, from the $21R$ points at $x=0.29$). The velocities are stated in units of 10^5 cm/sec.

Sound velocity	Lower limit (straight line)	Estimated (sine curve)	Measured[a]
Shear wave	7.00	7.24	7.25
Longitudinal	12.83	13.27	13.26

[a] Reference 15.

There is no reason to expect fine structure in the acoustic branches, which, in fact, do not deviate much from sine curves. Hence, one may obtain a lower limit for the acoustic velocities by joining the origin to the $21R$ points by straight lines. Alternatively, one may estimate the velocities by fitting sine curves through these points. Values obtained in both ways are given in Table V, together with the experimental values of Arlt and Schodder[15] for $6H$ SiC. The longitudinal velocity is stated in Ref. 15, and the shear velocity is obtained from the elastic constant data. Our experimental uncertainty in the energies of the $21R$ Raman lines is about 1%, so the agreement of estimated and experimental acoustic velocities to 0.1% in Table V is fortuitous.

VI. STRONG MODES AND ANISOTROPY

The strong modes of all polytypes, except cubic, have an angular variation (dependence on θ) like that reported in detail for $6H$ SiC in Table III of Ref. 2. The following statements apply to $4H$, $6H$, $15R$, and $21R$ SiC. The frequency of the E_{1t} (or E_t) mode, which is independent of θ, is found to be also independent of polytype at 797 cm^{-1}. It is plotted as TO_1 in Fig. 8. The other transverse mode has an angular dependence that may be taken as a measure of crystal anisotropy. The frequency of this mode, called TO_2, also depends on polytype. As θ is varied, the symmetry of this mode changes from A_{1t} at $\theta=90°$, with atomic motion along the c axis, through the mixed symmetry $(A_1+E)_t$, to part of the doubly degenerate E_1 (or E) at $\theta=0°$, with atomic motion perpendicular to the axis. The TO_2 frequencies were measured at two angles $\theta=45°$ and 90°, and are also plotted in Fig. 8. For convenience, a straight line is drawn through the two points from the known value, 797 cm^{-1}, at $\theta=0°$. Actually, the angular dependence is not linear,[2] but (TO_1-TO_2) at 45° is half that at 90°.

The longitudinal mode also has an angular variation. Like the transverse mode, its frequency is somewhat higher for atomic motion perpendicular to the c axis (E_{1t} or E_t at $\theta=90°$). Since the differences measured were only 1 to 3 cm^{-1}, and therefore comparable with experimental uncertainty, we could not establish a

[15] G. Arlt and G. R. Schodder, J. Acoust. Soc. Am. 37, 384 (1965).

TABLE VI. Anisotropy data for some SiC polytypes. The *hk* notation defines the "percent *h*" of atomic planes, with which the two measures of anisotropy, (TO_1-TO_2) and c_2/a, are correlated in Fig. 9.

Ramsdell notation	*hk* notation	Percent *h*	TO_1-TO_2 (cm^{-1})	c_2/a
3*C*	*k*	0	0	1.633
21*R*	*hkkhkkk*	29	8.6	
6*H*	*hkk*	33	9	1.6357[a]
15*R*	*hkhkk*	40	12.1	
4*H*	*hk*	50	14.8	
2*H*	*h*	100		1.641[b]

[a] Reference 18.
[b] Reference 17.

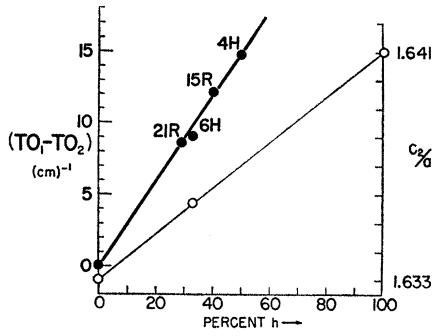

FIG. 9. Correlation with "percent *h*" of two measures of crystal anisotropy. The values of TO_1-TO_2 (filled circles and heavy line) are taken from Fig. 8. The c_2/a ratios (open circles and light line) are from x-ray measurements.

systematic dependence on polytype. For all polytypes, and for both $\theta=45°$ and 90°, the longitudinal-mode frequencies fall in the interval 967 to 971 cm^{-1}.

The results of a measurement on cubic SiC (zinc-blende structure) may also be reported here, since it has *only* strong modes accessible to Raman scattering. Because cubic SiC is isotropic, only two lines are found, TO at 796 ± 2 cm^{-1}, and LO at 972 ± 2 cm^{-1}.

Figure 8 gives one measure of crystal anisotropy, the frequency difference between TO_1 and TO_2 modes for $\theta=90°$. Another measure of anisotropy is the deviation of the c/a axial ratio[16] from the ideal 1.633. Accurate lattice constants have been reported in the literature[17,18] only for polytypes 2*H*, 6*H*, and cubic SiC. As indicated in Fig. 9, both measures of anisotropy are found to correlate with the percentage of "hexagonal" layers in the polytype stacking sequence, a percentage that is obtained from the *hk* notation of Table VI.

The *hk* notation is based on the fact that the inequivalent Si or C sites in the various polytypes are of only two kinds if the structure beyond second neighbors is disregarded. Each layer in a stacking sequence may then be considered to lie in a small hexagonal (*h*) or cubic (*k*) neighborhood, e.g., the layer *B* is *h* in the sequence *ABA*, but *k* in the sequence *ABC*. Zinc blende (all *k*) and wurtzite (all *h*) are the two end points of the series.

The *hk* scheme provides a simple and useful method of ordering the polytypes, even though it is based on a doubtful approximation. It has been used to correlate the SiC energy gaps,[19] and, for the ZnS polytypes, it has been used to correlate both energy gaps and birefringence.[20] The same ordering scheme[21] serves to correlate alloy structure and deviation from the ideal c/a ratio in certain rare-earth alloy systems[22] that form polytype structures,[23] and Hodges has discussed the theoretical basis of the correlation.[21]

The dependence of the TO_2 frequency on polytype is, of course, a deviation from a common SiC phonon spectrum. Since both lattice constants a and c_2 are functions of polytype, the TO_2 variation is related to the Grüneisen tensor for this mode. Other modes, no doubt, also have some frequency dependence on polytype for the same reason, but a 1% variation would not be apparent in Fig. 7.

[16] In first approximation, for any polytype, c is proportional to N, the number of layers in the stacking unit. To make a comparison of the small changes in c/a ratios, we first divide the polytype value of c by $\frac{1}{2}N$, to obtain the parameter c_2. This is the lattice constant for 2*H* SiC, and an average two-layer value for other polytypes.

[17] R. F. Adamsky and K. M. Merz, Z. Krist. **111**, 5 (1959).

[18] A. Taylor and R. M. Jones, in *Silicon Carbide*, edited by J. R. O'Connor and J. Smiltens (Pergamon Press, Inc., New York, 1960), p. 147.

[19] The correlation works well for polytypes discussed in Ref. 8, but fails to predict the 2*H* energy gap. This failure is considered in Lyle Patrick, D. R. Hamilton, and W. J. Choyke, Phys. Rev. **143**, 526 (1966).

[20] O. Brafman and I. T. Steinberger, Phys. Rev. **143**, 501 (1966).

[21] C. H. Hodges, Acta Met. **15**, 1787 (1967).

[22] I. R. Harris, C. C. Koch, and G. V. Raynor, J. Less-Common Metals **11**, 436 (1966).

[23] Although these metals have close-packed structures instead of tetrahedral, the possible stacking sequences are analogous (the same ABC sequences). The nomenclature used in the metallic systems is quite different, e.g., the names d. h. c. p. and Sm are used for the stacking sequences which we designate by the Ramsdell symbols 4*H* and 9*R*.